Superhydrophobic surface based on nano-engineering for enhancing durability of anti-corrosion

Yaya Zhou[1], Yibing Ma[1], Chunhong Qi[1], Luyan Shen[1], Qiang Fu[1, 2], Youyi Sun[1*], Yaqing Liu[1]

1.Shanxi Province Key Laboratory of Functional Nanocomposites, North University of China, Taiyuan 030051, P.R.China.

2.School of Civil and Environmental Engineering, University of Technology Sydney, Ultimo NSW 2007, Australia.

Abstract: Here, a new class superhydrophobic surface based on nano-engineering was proposed and prepared for improving the durability of corrosion protect. The durability of anticorrosion was evaluated by the Tafel polarization curves and electrochemical impedance spectroscopy under various environments, such as mechanical abrasion, chemical immersion and cool/thermal treatment. The superhydrophobic surface based on nano-engineering still showed excellent anticorrosion performance, such as low corrosion current (~10^{-10}A·cm^{-2}), large polarization resistance (>150.0MΩ·cm^2) and low corrosion rate (~10^{-6}mm/year). The good durability was attributed to the special nano-engineering,leading to low surface roughness and surface energy. The work provides a new method to improve durability of superhydrophobic surface for application in anticorrosion technology.

Keywords: Superhydrophobic surfaces; nano-engineering; surface energy; corrosion protection; durability.

Responding author: Fax: 86-351-3559669

E-mail address: syyi@pku.edu.cn (YY.Sun)

1.Introduction

Recently, superhydrophobic surfaces have received lots of attention as a promising solution to corrosion of metallic materials due to their superior water-repelling effects[1-2]. There were lots of works reporting the preparation, durability and anticorrosion of superhydrophobic surface, such as wet chemical reaction[3], etching[4], hydrothermal method[5], anodization[6], electrodeposition[7], sol-gel method[8], nanocomposite coating[9] and template method[10]. Most of these surfaces still showed low mechanical and chemical durability, in which their surface hydrophobicity could be easily reduced under external forces[11-15]. For example, superhydrophobic surface prepared by etching method showed low corrosion current of $1.61\times10^{-6}A\cdot cm^{-2}$. After 7 days of exposure, the superhydrophobicity was reduced, in which the water contact angle was less than 150.0^{o}[11]. A new superhydrophobic textured steel surface was fabricated by a simple and rapid method to enhance anti-corrosion properties of S45C steel substrate, which also showed low corrosion current of $1.65\times10^{-6}A\cdot cm^{-2}$. After abrasion for 50.0cm, the contact angle of superhydrophobic surface was reduced from 158.0^{o} to 151.0^{o}[12]. A new superhydrophobic surface was fabricated on AZ91D magnesium alloy through a process combining both electrodeposition and chemical modification. The superhydrophobic surface exhibited excellent anticorrosion of $1.96\times10^{-8}A\cdot cm^{-2}$. After mechanical abrasion for 500.0mm, the contact angle of superhydrophobic surface was decreased from 163.3^{o} to 150.0^{o}. After immersion in NaOH solution for 24.0h, the contact angle of superhydrophobic surface was decreased from 163.3^{o} to 124.0^{o}[13]. The poor durability of traditional superhydrophobic surface was due to its highly porous micro-structures or hierarchical structure, which was easily damaged by

external forces, resulting in a decease of anticorrosion. It is still high challenge to improve to durability of anticorrosion for the superhydrophobic surface.

Here, a new superhydrophobic surface based on nano-engineering was proposed and prepared by a facile method. The durability of superhydrophobic surface based on nano-engineering was investigated and evaluated under mechanical abrasion, thermal/cooling treatment and chemical solution immersion. The superhydrophobic surface exhibited excellent durability, which was attributed to surface nano-engineering with low surface roughness and surface energy.

2. Experimental

2.1 Materials

All chemicals were analytical reagent grade and used as raw materials without further purification. Iron (III) chloride hexahydrate ($FeCl_3 \cdot 6H_2O$), iron(II) chloride tetrahydrate ($FeCl_2 \cdot 4H_2O$), and sodium hydroxide (NaOH), ammonia solution ($NH_3 \cdot H_2O$), ethyl silicate (TEOS), urea, 1-amyl alcohol, cyclohexane, toluene, ethanol (C_2H_5OH), acetone and hydrochloric acid (HCl) were purchased from Tianjin guangfu technology. N-octyl triethoxysiloxane were purchased from Aladdin. Epoxy and curing agent were purchased from Shanghai YueKe Composite Co., Ltd. Q235 was purchased from the local chemical market.

2.2 Preparation of superhydrophobic surface based on nano-engineering

The superhydrophobic surface based on nano-engineering was prepared by a two-step method as shown in Scheme 1. Firstly, the Fe_3O_4@SiO_2@OTS nanoparticles with low surface energy were synthesized as shown in following. The 5.0g NaOH, 3.6g $FeCl_2 \cdot 4H_2O$ and 6.1g $FeCl_3 \cdot 6H_2O$ were dissolved in the 90.0mL deionized water. 92.5mL NaOH solution (54.0mg/mL) was added to above mixture under stirring at 50.0℃. The above mixing solution was reacted for 90.0min. The Fe_3O_4 nanoparticle

was separated by the magnet from the reaction solution and further dispersed in ethanol/water mixing solution (4:1). 5.0mL ammonia and 2.0mL TEOS were added to above 125.0mL Fe_3O_4 nanoparticles dispersion solution (8.0mg/mL) and was mechanically stirred for 60.0min to form Fe_3O_4@SiO_2 nanoparticles. The Fe_3O_4@SiO_2 nanoparticles were also separated by the magnet from the reaction solution. The Fe_3O_4@SiO_2 nanoparticles were washed by the ethanol solution and further dispersed in toluene solution. 20.0mL N-octyl trimethylsilyl (OTS) was added to 50.0mL toluene solution (0.2g/mL). The above mixing solution was reacted at 120.0℃ for 20.0h to form Fe_3O_4@SiO_2@OTS. The Fe_3O_4@SiO_2@OTS was separated by magnet and further dispersed in ethanol. Secondly, the superhydrophobic surface based on dual-layer structure was prepared by the spraying method as shown in following. 20.0g bisphenol A type epoxy resin and 4.0g amine curing agent (5:1) was mixed and sprayed on the surface of iron metal (Q235), The epoxy coating was cured at 80.0° for 45.0 minutes. Then, the Fe_3O_4@SiO_2@OTS dispersion ethanol was sprayed on the surface of epoxy coating, Finally, the composite coating was further treated at 80.0℃ for 20.0h.

Scheme 1.

2.3 Structure characterization

The structure of materials was identified by powder X-ray diffraction (XRD, Smartlab (3), Rigaku, Japan) with Cu Kα radiation diffraction (λ =0.154nm, operating voltage 35.0kV, current 40.0mA) in the scan range 5-80°, scanning speed 4° min^{-1}.

The micro-structure of materials was observed by Field emission scanning electron microscopy (SEM, JEOL, JSM-6701F) and a Nanovea ST400 non-contact white light profilometer (Nanovea, Irvine, CA, USA).

2.4 Superhydrophobic performance

Bounce phenomenon was characterized by Krüss DSA 100 (Krüss, Germany) apparatus with high-speed camera, Japan KEYENCE). The auto video record of bouncing phenomena was recorded by setting the time sequence of 0.02s for each frame to the end of droplet stability.

Water contact angle and surface energy test was characterized by Krüss DSA 100 (Krüss, Germany) apparatus for 3.0 times at 5.0 different places for each sample with the volume of water drop of 10.0μl. In addition, the Krüss DSA 100 (Krüss, Germany) apparatus was also used to test the contact angle (CA) at 5.0 different places for each sample with polar liquid (H_2O) and non-polar liquid (CH_2I_2) to obtain surface energy. Then, the surface energy (γ_s , mN/m) could also be calculated by Girfalco-Good-Fowkes-Young[16-17].

$$\gamma_L(1+\cos\theta) = 2\left(\gamma_S^D\gamma_L^D\right)^{1/2} + 2\left(\gamma_S^P\gamma_L^P\right)^{1/2}$$
$$\gamma_S = \gamma_S^D + \gamma_S^P$$

Where γ_L is surface tension of the sample（γ_L(H_2O) =72.8mN/m and γ_L(CH_2I_2) =50.8mN/m), θ is the water contact angle of the liquid; γ_S is the surface free energy of a solid substrate, γ_L^D and γ_L^P is the color dispersion part and the polar part of the liquid surface tension, (γ_L^D(H_2O)=21.8mN/m, γ_L^P(H_2O)=51.0mN/m, γ_L^D(CH_2I_2)=21.8 mN/m, γ_L^P (CH_2I_2) =51.0mN/m)

2.5 Mechanical stability and adhesive properties

The mechanical stability of superhydrophobic surface was evaluated by sandpaper abrasion test. The superhydrophobic surface was moved on a 240# SiC abrasive paper in one direction under a standard weight of 100.0g for 10.0cm. The 100 abrasion cycles were carried out at the same process.

The adhesion force measurement of the coating was performed according to ASTM 3359-2002. In addition, Using a standard cross-cut tester kit (QFH, from Lambert, Guangzhou, China) to draw vertically on the surface of the superhydrophobic coating~~the scratch test was performed by a standard cross-cut tester kit (QFH, from Lambert, Guangzhou, China)~~ to examine the effect of deep mechanical damage on water repellant properties. The force should be uniform and stable when drawing the grid, so that the cutting edge can just penetrate the coating and touch the base during cutting, and then gently brush the chip off with a brush (GB/T 9286-1998).

2.6 Thermal/cooling stability

The thermal/cooling stability test was performed on the constant temperature and humidity box (QTH-600G, China Guangdong) in 3.5wt% NaCl solution at 60℃ or -20℃ for 10 days.

2.7 Anticorrosion performance

(1) Electrochemical measurements

The anticorrosion performance was characterized by the Tafel polarization and electrochemical impedance spectroscopy (EIS) measurements on an electrochemical workstation (CHI660C, Chenhua, Shanghai). In a three-electrode system, the superhydrophobic surface coated metal (carbon steel), platinum plate and Hg/HgO electrode (SCE) were directly used as the working electrode, the counter and reference electrode, respectively. The corrosion current density (I_{corr}) and the corrosion potential (E_{corr}) were obtained by using electrochemical analyzer software. The polarization resistance (R_p) was determined from Tafel plots by using the Stern-Geary equation[18-20]：

$$Rp = \frac{b_a \times b_c}{2.303 Icorr\left(b_a + b_c\right)}$$

b_a and b_c is the slope of anodic and cathodic Tafel plots, respectively.

$$V_{corr} = \frac{A \cdot i_{corr}}{n\rho F} \times 87600 (mm/year)$$

The EIS results were analyzed by using Zsimpwin software and fitting the Nyquist through the equivalent circuit, the Rct and CPE were obtained[21]. The corrosion rate (V_{corr}, mm/year) was obtained by the following equation[22]:

Where the formula weight (A) is 55.85g/mol, and the density (ρ) is 7.85g/cm^3 for metal, the chemical valence (n) is 2 for Fe and F is the Faraday constant (F=96485C/moL).

(2) Corrosion immersion

The immersion corrosion test was performed on a KD-60F type immersion corrosion tester in 3.5±0.5wt% NaCl solution, acid solution (pH=1) and alkali solution (pH=14) for 20.0 days, respectively.

3. Results and discussion

The formation of Fe_3O_4@SiO_2@OTS composite nanoparticles was firstly confirmed by the XRD and IR as shown in Fig.1A and Fig.1B, respectively. As shown in Fig.1A, it clearly showed some strong diffraction peaks at 2θ=18.2°、29.9°、35.4°、37.1°、43.0°、53.3°、56.9°、62.6°and 74.1°, which were assigned to the (111) , (220), (311), (400), (422), (511), (440), and (533) planes of Fe_3O_4 (JCPDS card, file no. 79-0418)[14, 18-20]. An additional broad peak at 21.5° was assigned to the amorphous silica oxide[19]. Fig.1B shows the IR of Fe_3O_4@SiO_2@OTS composite nanoparticles. The peak of 571.0cm^{-1} was attributed to Fe-O bond of Fe_3O_4. In addition, the strong absorption peaks at 466.0cm^{-1}, 801.0cm^{-1}, 968.0cm^{-1}, 1096.0cm^{-1} and 1632.0cm^{-1} were attributed to the vibration of Si-O-H bending, Si-O-Si stretching

and H-O-H bending vibration of SiO_2@OTS, respectively[23-24]. The absorption peaks at 2920.5cm^{-1} and 2849.0cm^{-1} were attributed to the CH_2 asymmetric stretching mode of OTS. These results confirmed that the composition of Fe_3O_4, SiO_2 and OTS all presented in the composite nanoparticles. The micro-structure of composite nanoparticles was further characterized by the SEM images. Fe_3O_4 nanoparticles showed uniform size of ca.40.0nm and uniformly spherical shape as shown in Fig.1C. After coating with SiO_2, the size of composite nanoparticles obviously increased to ca. 90.0nm as shown in Fig.1D. The change of size further confirmed that the SiO_2 was coated on surface of Fe_3O_4 nanoparticles, in which the thickness of SiO_2 shell was about 25.0nm. The above result was further confirmed by the TEM image as shown in Fig.1E. It clearly showed spherical shape with core-shell structure. The surface energy of Fe_3O_4@SiO_2@OTS composite nanoparticles was displayed in inset of Fig.1C and 1D, in which the surface energy (5.9mN/m) was calculated by the Girfalco-Good-Fowkes-Young. These results indicated the formation of Fe_3O_4@SiO_2@OTS composite nanoparticles with low surface energy, which was key role for the preparation of superhydrophobic surface based on nano-engineering.

Fig.1.

Here, a new class superhydrophobic surface based on nano-engineering was proposed, resulting from assemblies of nanoparticles under adhesion of epoxy resin as shown in Fig.2A. As shown in Fig.2B, the pure EP coating clearly showed transparent film. After covered with Fe_3O_4@SiO_2@OTS composite nanoparticles, the EP film changed from transparency to brown yellow. Furthermore, the brown yellow was uniform distribution. The result indicated that the nanoparticles were uniformly covered on surface of pure EP coating. Fig.2C shows the XRD patterns of pure EP and Fe_3O_4@SiO_2@OTS/EP coated-metal. For the pure EP coating, it clearly showed a

strong and wide diffraction peak at 18.0°, which was assigned to the non-crystalline characteristic diffraction peak of EP. In addition to above diffraction peak, the XRD patterns of Fe_3O_4@SiO_2@OTS/EP clearly showed some new peaks at 2θ=30.1°, 35.5°,43.1°, 53.7°, 57.2°and 62.8, which were indexed to (311), (400), (422), (511), (440) and (533) plane of Fe_3O_4, respectively[25]. These results confirmed the formation of coating based on Fe_3O_4@SiO_2@OTS composite nanoparticles. The inset of Fig.2B shows the digital image of water droplets on pure EP and Fe_3O_4@SiO_2@OTS/EP coating. The water droplets on EP coating and Fe_3O_4@OTS-SiO_2/EP coatings were hemisphere and complete sphere, respectively. These results indicated that Fe_3O_4@SiO_2@OTS/EP coating exhibited good superhydrophobicity.

Fig.2.

Surface morphology of Fe_3O_4@SiO_2@OTS/EP coating was characterized by SEM images and non-contact white light profilometer as shown in Fig.3. As for the pure EP coating (in Fig.3A), a flat and smooth surface was observed. For Fe_3O_4@SiO_2@OTS/EP (Fig.3B), some nanoparticles were clearly covered on surface of EP coating, forming nano-engineering. The above result was further confirmed by the 3D optical profilometry surface image as shown in Fig.3C. The low surface roughness of ca. 220nm was observed(the standard deviation for the surface roughness of the superhydrophobic coating is 1.33), which was far smaller than that of superhydrophobic surface reported in previous works[26-29]. The result further confirmed the formation of nano-engineering on surface of Fe_3O_4@SiO_2@OTS/EP coating. Although it showed nano-engineering with low surface roughness, the Fe_3O_4@SiO_2@OTS/EP coating still exhibited large water contact angle (170.0°), indicating good superhydrophobicity. The result was mainly attributed to low surface

energy of nano-engineering, resulting from surface modification of OTS.

Fig.3.

The superhydrophobicity of Fe_3O_4@SiO_2@OTS/EP coating was further investigated by a more realistic study of the bounce phenomenon. A high-speed camera (Japan KEYENCE) with a frame rate of 1000/s was used to record the bounce of 10.0μl droplet falling to surface of Fe_3O_4@SiO_2@OTS/EP as shown in Fig.4. As well-known, when water droplets were fallen to the superhydrophobic surface, the water droplets tended to bounce instead of wetting the surface. As shown in Fig.4, it displayed the approach, contact, deformation and departure of the water droplet from surface of Fe_3O_4@SiO_2@OTS/EP in the bouncing test. In the process, the droplet did not fragment into small pieces, and no anchoring points with residual water was observed. The result further confirmed good superhydrophobicity of Fe_3O_4@SiO_2@OTS/EP coating with surface nano-engineering.

Fig.4.

The adhesion between Fe_3O_4@SiO_2@OTS/EP coating and metal substrate was further evaluated by the scratch-test method as shown in Fig.5. It clearly showed that the Fe_3O_4@SiO_2@OTS/EP coating was few damaged after mechanical scratches as shown in Fig.5A, which was assigned to 0 class according to standard of scratch-test method [30]. The result confirmed the good adhesion of Fe_3O_4@SiO_2@OTS/EP coating, indicating a good mechanical stability. The good adhesion was attributed to special structure of nano-engineering with low surface roughness, in which the nanoparticles was adhered on surface of substrate by epoxy resin. Furthermore, the nano-engineering after scratch-test still showed good superhydrophobicity as shown in Fig.6C, in which the water droplet was complete sphere and water contact angle

was about 170.0^{o}. The result further confirmed the good mechanical stability and superhydrophobicity of nano-engineering.

Fig.5.

As well-known, corrosion medium was based on aqueous acid, alkaline, or salt solutions[19, 23, 31]. So, the durability of superhydrophobic surface based on nano-engineering was firstly evaluated under acid, alkali and 3.5wt% NaCl aqueous solutions. Fig.6A shows the Tafel polarization curves of superhydrophobic surface coated-metal before and after immersion in acid, alkali and 3.5wt% NaCl aqueous solutions for 10 days. All Tafel polarization curves were slight shift to a negative direction after immersion in chemical solutions. In addition, the I_{corr} of superhydrophobic surface coated-metal slightly increased after immersion in chemical aqueous solutions for 10 days. Fig.6B shows the Nyquist plots of superhydrophobic surface coated-metal before and after immersion in chemical aqueous solutions for 10 days, respectively. All samples clearly showed similar Nyquist plots. And the charge transfers resistance (R_{ct})—also slightly decreased for superhydrophobic surface coated-metal after immersion in chemical solution for 10 days. Yet, it was still showed lower I_{corr} and larger R_{ct} comparing to previous works [18-20, 32-34]. As well-known, the lower I_{corr} showed slower corrosion rate and the larger R_{ct} showed more difficult diffusion of ion from solution to metal[34], leading to a better anticorrosion performance. These results indicated that present superhydrophobic surface based on nano-engineering exhibited good durability for application in anticorrosion under acid, alkali and 3.5wt% NaCl aqueous solutions.

Fig.6.

The anticorrosion of superhydrophobic surface based on nano-engineering as function of abrasion cycles was also investigated by Tafel polarization curves and

electrochemical impedance spectroscopy as shown in Fig.7. As shown in Fig.7A, the Tafel polarization curves of superhydrophobic surface coated-metal plate under 0, 50^{th} and 100^{th} abrasion cycle was characterized and compared. The I_{corr}, E_{corr}, R_p and V_{corr} were calculated and concluded in Table 1. The I_{corr} of superhydrophobic surface-coated metal after 0, 50^{th} and 100^{th} abrasion cycle was about $2.6\times10^{-11}A\cdot cm^{-2}$, $4.3\times10^{-10}A\cdot cm^{-2}$ and $5.3\times10^{-10}A\cdot cm^{-2}$, respectively. The Nyquist plots of superhydrophobic surface-coated metal were also characterized as shown in Fig.7B. The high-frequency semicircle slightly decreased with increasing in abrasion cycle. It clearly showed that the R_{ct} of superhydrophobic surface-coated metal was reduced from $167.1M\Omega\cdot cm^2$ to $121.8\ M\Omega\cdot cm^2$ after 100^{th} abrasion cycle. The I_{corr} and R_{ct} after 100^{th} abrasion cycle were still lower and larger more than two orders of magnitude comparing to previous works, respectively[24, 27-33]. The corresponding equivalent electrical circuit model of superhydrophobic surface coated-metal was also described as shown in inset of Fig.7B. R_s, R_{ct} and *CPE* represented the solution resistance, charge transfer resistance and the capacitance of the electrical double layer, respectively[35-37]. In addition, there was a slight change in slide angle and water contact angle as shown in Table 1. These results confirmed the good mechanical durability of superhydrophobic surface for corrosion protect.

Fig.7.

Table 1.

The durability of superhydrophobic surface based on nano-engineering was also investigated under various temperatures as shown in Fig.8. Fig.8A shows the Tafel polarization curves of superhydrophobic surface-coated metal before and after thermal or cooling treatment for 10 days. The Tafel polarization curve of superhydrophobic surface-coated metal was slight and few shift to a negative

direction after thermal and cooling treatment for 10 days. As expected, the I_{corr} of superhydrophobic surface-coated metal also slightly increased after thermal or cooling treatment for 10 days as shown in Table 2. Fig.8B shows the Nyquist plots of superhydrophobic surface-coated metal before and after thermal or cooling treatment for 10 days. The high-frequency semicircle of superhydrophobic surface-coated metal also slightly decreased after thermal or cooling treatment for 10 days, in which the R_{ct} was reduced from 167.8MΩ·cm^2 to 156.1MΩ·cm^2. These results confirmed the durability of superhydrophobic surface based on nano-engineering for corrosion protect under thermal and cooling environment.

Fig.8.

Table 2.

It was well-known that the good corrosion protection of superhydrophobic surface was mainly attributed to formed air film[38-40]. However, air film failed within hours and rarely for days[41-42], leading to a poor durability of anticorrosion[41-44]. Here, stability of air films on superhydrophobic surface based on nano-engineering was also investigated as function of days as shown in Fig.9. As shown in Fig.9A-C, the air film was retained in acid, alkali and NaCl aqueous solutions for more than 10 days. Furthermore, the air film was still observed after 100 abrasion cycles and thermal/cooling treatment for 10 days as shown in Fig.9D-F. These results suggested that the good durability of superhydrophobic surface based on nano-engineering was due to the good stability of formed air film. By comparing with the anticorrosion of other superhydrophobic surfaces as shown in Table 3, present superhydrophobic surface showed best anticorrosion performance. The result was attributed to special nano-engineering with low surface roughness as shown in Scheme 2. The water could not penetrate the air barrier under flowing and washing

force after prolonged immersion and a Cassie contact was remained for long time. In a comparison, the water easily penetrated into superhydrophobic surface with large surface roughness, resulting from hierarchical porous or array structures [43-44]. In addition to this, the EP film also effectively retarded the diffusion of ionic and oxygen in water into metal substrate as shown in Scheme 2.

Scheme 2.

4. Conclusions

In summary, a new class superhydrophobic surface based on nano-engineering was prepared by a simple spraying method. It exhibited excellent durability for application in corrosion protect of metal under chemical immersion, mechanical, and thermal/cooling environment. The result was attributed to nano-engineering with low surface energy. The work provides a new method to improve the durability of superhydrophobic surface for application in long-lasting anticorrosion.

Acknowledgments

The authors are grateful for the support of National Natural Science Foundation of China under grants (51773184 and U1810114), and Shanxi Provincial Natural Science Foundation of China (201701D121046 and 201803D421081).

References

[1]R.M.N.M. Rathnayake, M.M.M.G.P.G.Mantilaka, MasanoriHaracHsin-HuiHuang, H.W.M.A.C.Wijayasinghe, M.Yoshimura, H.M.T.G.A.Pitawala. Graphite intercalated polyaniline composite with superior anticorrosive and hydrophobic properties, as protective coating material on steel surfaces. Applied Surface Science. 2017, 15: 445-453.

[2]P. Wang, D. Zhang, R. Qiu, J.J. Wu, Y. Wan. Super-hydrophobic film prepared on zinc and its effect on corrosion in simulated marine atmosphere. Corrosion Science. 2013, 69: 23-30.

[3]A. Chaudhary, H.C. Barshilia. Nanometric Multiscale Rough CuO/$Cu(OH)_2$ Superhydrophobic Surfaces Prepared by a Facile One-Step Solution-Immersion Process: Transition to Superhydrophilicity with Oxygen Plasma Treatment. J. Phys. Chem. C. 2011, 115: 18213-18220.

[4]Z. Yang, X.P. Liu, Y.L. Ti, Insights into the wettability transition of nanosecond laser ablated surface under ambient air exposure. Journal of Colloid and Interface Science. 2019, 533: 268-277.

[5]Y.L. Shi, W. Yang, X.J. Feng, Y.S. Wang, G.R. Yue. Fabrication of superhydrophobic ZnO nanorods surface with corrosion resistance via combining thermal oxidation and surface modification. Materials Letters. 2015, 151: 24-27.

[6]H. Saffari, B. Sohrabi, M.R. Noori, H.R.T. Bahrami. Optimal condition for fabricating superhydrophobic Aluminum surfaces with controlled anodizing processes. Applied Surface Science. 2018, 435: 1322-1328.

[7]J.J. Conde, P.F. Aparicio, A.M. Chaparro. anti-corrosion coating for metal surfaces based on superhydrophobic electrosprayed carbon layers. Applied Materials Today. 2018, 13: 100-106.

[8]X.F. Zhang, R.J. Chen, Y.H. Liu, J.M.Hu. Electrochemically generated sol-gel films as inhibitor containers of superhydrophobic surfaces for the active corrosion protection of metals. J. Mater. Chem. A. 2016, 4: 649-656.

[9]B. Ge, L. Han, X. Liang, F.Y. Li, X.P. Pu, X.T. Zhu, Z.Z. Zhang, X. Shao, C.Y. Jin, W.Z. Li. Fabrication of superhydrophobic Cu-BiOBr surface for oil/water separation and water soluble pollutants degradation. Applied Surface Science. 2017, 410:

445-453.

[10]B.P. Zhou, Y.B. Gao, Y.Y. Mao, W.J. Wen. Facile preparation of superhydrophobic PDMS with patternable and controllable water adhesion Characteristics. J. Mater. Sci. 2017, 52: 11428-11441.

[11]S.J. Yuan, S.O. Pehkonen, B. Liang, Y.P. Ting, K.G. Neoh, E.T. Kang. Superhydrophobic fluoropolymer-modified copper surface via surface graft polymerisation for corrosion protection. Corrosion science. 2011, 53(9): 2738-2747.

[12]H.M. Zhang, J. Yang, B.B. Chen, C. Liu, M.S Zhang, C.S. Li. Fabrication of superhydrophobic textured steel surface for anti-corrosion and tribological properties. Applied Surface Science. 2015, 359: 905-910.

[13]Z.X. She, Q. Li, Z.W. Wang, L.Q. Li, F.N. Chen, J.C. Zhou. Researching the fabrication of anticorrosion superhydrophobic surface on magnesium alloy and its mechanical stability and durability. Chemical Engineering Journal. 2013, 228: 415-424.

[14]Z.Q. Yang, L.D. Wang, W. Sun, S.J. Li, T.Z. Zhu, W. Liu, G.C. Liu. Superhydrophobic epoxy coating modified by fluorographene used for anti-corrosion and self-cleaning. Applied Surface Science. 2017, 401: 146-155.

[15]Y.Y. Zhou, Y.B. Ma, Y.Y. Sun, Z.Y. Xiong, C.H. Qi, Y.H. Zhang, Y.Q. Liu. Robust Superhydrophobic Surface Based on Multiple Hybrid Coatings for Application in Corrosion Protection. ACS Appl. Mater. Interfaces. 2019, 11: 6512-6526.

[16]A. Baldan. Adhesion phenomena in bonded joints. International Journal of Adhesion and Adhesives. 2012, 38: 95-116.

[17]F.M. Fowkes. Attractive forces at interfaces. Industrial & Engineering Chemistry 1964, 56: 40-52.

[18]Z.Q. Qian, S.D. Wang, X.S. Ye, Z. Liu, Z.J. Wu. Corrosion resistance and wetting

properties of silica-based superhydrophobic coatings on $AZ_{31}B$ Mg alloy surfaces. Applied Surface Science. 2018, 453: 1-10.

[19]S.Cui, S.X.Lu, W.G.Xu, B.F.An, B.Wu. Fabrication of robust gold superhydrophobic surface on iron substrate with properties of corrosion resistance, self-cleaning and mechanical durability. Journal of Alloys and Compounds. 2017, 728: 271-281.

[20]L.S.Zhang, Y. Jiang, W.Zai, G.Y. Li, S.C. Liu, J.S. Lian, Z.H. Jiang. Fabrication of Superhydrophobic Calcium Phosphate Coating on Mg-Zn-Ca alloy and Its Corrosion Resistance. Journal of Materials Engineering and Performance. 2017, 26: 6117-6129.

[21]F.Peng, D.Wang, X.Ma, H.Zhu, Y.Qiao, X.Liu. Advances in Metallic Biomaterials “Petal Effect” -Inspired Superhydrophobic and Highly Adhesive Coating on Magnesium with Enhanced Corrosion Resistance and Biocompatibility. 2018, 61: 629-642.

[22]D.H. Zhang, D.J. Kong. Surface and cross-section characteristics and immersion corrosion behavior of laser thermal sprayed amorphous $AlNiCoCrY_2O_3$ coatings. Applied Surface Science. 2018, 457: 69-82.

[23]G.S.An, D.H.Chae, J.U.Hur, A.H.Oh, H.H.Choi, S.C.Choi, Y.S.Oh, Y.G.Jung. Hollow-structured $Fe_3O_4@SiO_2$ nanoparticles: Novel synthesis and enhanced adsorbents for purification of plasmid DNA. Ceramics International. 2018, 44: 18791-18795.

[24]S.Dey, S. Chatterjee, B.P.Singh, S. Bhattacharjee, T.K.Rout, D.K.Sengupta, L. Besra. Development of superhydrophobic corrosion resistance coating on mild steel by electrophoretic deposition. Surface and Coatings Technology. 2018, 341: 24-30.

[25]Z.Chen, L.M. Hao, A.Q.Chen, Q.J. Song, C.L.Chen. A rapid one-step process for fabrication of superhydrophobic surface by electrodeposition method. Electrochimica Acta. 2012, 59: 168-171.

[26]H.Alamri, A.Al-Shahrani, E. Bovero, T. Khaldi, G. Alabedi, W. Obaid, I. Al-Taie, A. Fihri. Self-cleaning superhydrophobic epoxy coating based on fibrous silica-coated iron oxide magnetic nanoparticles. Journal of colloid and interface science. 2018, 513: 349-356.

[27]D. Jiang, H.Zhou, S.Wan, G.Y.Cai, Z.H.Dong. Fabrication of superhydrophobic coating on magnesium alloy with improved corrosion resistance by combining micro-arc oxidation and cyclic assembly. Surface and Coatings Technology. 2018, 339: 155-166.

[28]R.Zandipak, S.Sobhanardakani. Novel mesoporous Fe_3O_4/SiO_2/CTAB-SiO_2 as an effective adsorbent for the removal of amoxicillin and tetracycline from water. Clean Technologies and Environmental Policy. 2018, 1-15.

[29]C.Anitha, S.Syed Azim, S.Mayavan. Influence of particle size in fluorine free corrosion resistance superhydrophobic coating-Optimization and stabilization of interface by multiscale roughness. Journal of Alloys and Compounds. 2018, 765: 677-684.

[30]E.Aslani, A.Abri, M. Pazhang. Immobilization of trypsin onto Fe_3O_4@SiO_2-NH_2 and study of its activity and stability. Colloids and surfaces B Biointerfaces 2018, 170: 553-62.

[31]B.Wu, S.X.Lu, W.G.Xu, S.Cui, J.Y.Li, P.F.Han. Study on corrosion resistance and photocatalysis of cobalt superhydrophobic coating on aluminum substrate. Surface and Coatings Technology 2017, 330: 42-52.

[32]X.K.Cui, G.Y.Zhu, Y.F.Pan, Q.Shao, C.Zhao, M.Y.Dong, Y.Zhang, Z.H.Guo.

Polydimethylsiloxane-titania nanocomposite coating: Fabrication and corrosion resistance. Polymer. 2018, 138: 203-210.

[33]Y.W.Ye, Z.Y.Liu, W.Liu, D.W.Zhang, H.C.Zhao, L.P.Wang, X.G.Li. Superhydrophobic oligoaniline-containing electroactive silica coating as pre-process coating for corrosion protection of carbon steel. Chemical Engineering Journal. 2018, 348: 940-951.

[34]Q.Ma, Z.Tong, W.Wang, G.G.Dong. Fabricating robust and repairable superhydrophobic surface on carbon steel by nanosecond laser texturing for corrosion protection. Applied Surface Science. 2018, 455: 748-757.

[35]J.R.Yao, Y.Y.Sun, Y.Wang, Q.Fu, Z.Y.Xiong, Y.Q.Liu. Magnet-induced aligning magnetorheological elastomer based on ultra-soft matrix. Composites Science and Technology. 2018, 162: 170-179.

[36]C.B.Liu, S.H. Qiu, P. Du, H.C. Zhao, L.P. Wang. An ionic liquid–graphene oxide hybrid nanomaterial: synthesis and anticorrosive applications. Nanoscale. 2018, 10: 8115-8124.

[37]S.G.Zhou, Y.M.Wu, W.J.Zhao, J.J.Yu, F.W.Jiang, L.Q.Ma. Comparative corrosion resistance of graphene sheets with different structures in waterborne epoxy coatings. Colloids and Surfaces A: Physicochemical and Engineering Aspects. 2018, 556: 273-283.

[38]D.Y.Yu, J.T.Tian, J.H.Dai, X.Wang. Corrosion resistance of three-layer superhydrophobic composite coating on carbon steel in seawater. Electrochimica Acta. 2013, 97: 409-419.

[39]C.Q.Wu, Q.Liu, J.Y. Liu, K.B.Takahashi, R.Chen, L.H.Liu, R.M.Li, P.L.Liu, J.Wang. Hierarchical flower like double-layer superhydrophobic films fabricated on AZ31 for corrosion protection and self-cleaning. New Journal of Chemistry. 2017, 41:

12767-12776.

[40]M.C.Xu, G.Y.Sun, C.J.Kim. Infinite lifetime of underwater superhydrophobic states. Physical review letters. 2014, 113: 136103.

[41]L.Jiang, Y.Zhao, J.Zhai. A lotus-leaf-like superhydrophobic surface: a porous microsphere/nanofiber composite film prepared by electrohydrodynamics. Angewandte Chemie. 2004, 116: 4438-4441.

[42]W.Barthlott, T.Schimmel, S.Wiersch, K.Koch, M.B.Matthias Barczewski, S.Walheim, A.Weis, A. Kaltenmaier, A. Leder Holger F. Bohn. The Salvinia paradox: superhydrophobic surfaces with hydrophilic pins for air retention under water. Advanced Materials. 2010, 22: 2325-2328.

[43]Y. Li, W.P. Cai, B.Q. Cao, G.T. Duan, F.Q. Sun, C.C.Li, L.C.Jia. Two-dimensional hierarchical porous silica film and its tunable superhydrophobicity. Nanotechnology. 2005, 17: 238.

[44]P.A.Levkin, F.Svec, J.M.J. Fréchet. Porous polymer coatings: a versatile approach to superhydrophobic surfaces. Advanced Functional Materials. 2009, 19: 1993-1998.

Table 1. Analysis results of Tafel polarisation curves and electrochemical impedance spectroscopy of the superhydrophobic surface under 0, 50^{th} and 100^{th} abrasion cycle.

Table 2. Analysis results of Tafel polarisation curves and electrochemical impedance spectroscopy of the superhydrophobic surface under thermal/cooling treatment for 10 days.

Table 3. Analysis results of Tafel polarisation curves and electrochemical impedance spectroscopy of superhydrophobic surface coated-metal before and after immersion in acid, alkali and NaCl aqueous solutions.

Scheme 1. Preparation process of superhydrophobic surface based on low surface energy.

Scheme 2. Schematic illustration of anticorrosion mechanism of (A) conventional polymer coating and (B) superhydrophobic surface.

Fig.1. (A) XRD and (B) IR of Fe_3O_4@SiO_2@OTS, SEM image of (C) pure Fe_3O_4, (D) Fe_3O_4@SiO_2@OTS, (E) TEM image of Fe_3O_4@SiO_2@OTS, the inset of (C) and (D) is CH_2I_2 and water contact angle on surface of Fe_3O_4@SiO_2@OTS, respectively.

Fig.2. (A) Schematic superhydrophobic surface based on low surface energy, (B) optical photograph and (C) XRD of (a) pure EP and (b) Fe_3O_4@SiO_2@OTS/EP

coated-metal, (D) the optical photo of cross section of Fe_3O_4@SiO_2@OTS/EP. The inset of (B) is the corresponding digital image of water droplets on the as-prepared surface.

Fig.3. SEM images of (A) pure EP and (B) Fe_3O_4@SiO_2@OTS/EP coated-metal. (C) 3D optical profile of Fe_3O_4@SiO_2@OTS/EP coated-metal. The inset of (A) and (B) is the corresponding digital image of corresponding water contact angle.

Fig.4. The sequential digital images of a water droplet during the bouncing test on the superhydrophobic surface (the orange arrows indicate the directions of the water droplet moving).

Fig.5.Optical photograph of (A) Fe_3O_4@SiO_2@OTS/EP coated-metal after mechanical scratches, (B)pure EP, and (C) digital image of water droplets on superhydrophobic surface coated-metal after mechanical scratches. The inset of (C) is the digital image of water contact angles on surface of Fe_3O_4@SiO_2@OTS/EP after mechanical scratches.

Fig.6. (A)Tafel polarization curves and (B) Nyquist plots of superhydrophobic surface coated-metal (a) before and after immersion in (b) acid, (c) alkali and (d) 3.5wt% NaCl aqueous solutions.

Fig.7. (A) Tafel polarization curves and (B) Nyquist plots of superhydrophobic surface coated-metal after (a) 0, (b) 50^{th} and (c) 100^{th} abrasion cycle. The inset of (B) is the corresponding equivalent electrical circuit model of Fe_3O_4@SiO_2@OTS/EP coated- metal.

Fig.8. (A) Tafel polarization curves and (B) Nyquist plots of superhydrophobic surface-coated metal (a) before and after (b) thermal or (c)cooling treatment for 10 days.

Fig.9. Optical photograph of superhydrophobic surface coated-metal immersion in (A)

acid solution (pH=1.0), (B) alkali solution (pH=14.0), (C) NaCl solution (3.5wt%) for 10 days. Optical photograph of superhydrophobic surface coated-metal after (D) thermal and (E) cooling treatment for 10 days immersion in NaCl water (3.5wt%). (F) Optical photograph of superhydrophobic surface coated-metal after 100 abrasion cycles immersion in NaCl solution (3.5wt%).

Table 1.

Abrasion cycle	E_{corr} (V)	I_{corr} ($A \cdot cm^{-2}$)	R_p ($M\Omega\ cm^2$)	R_{ct} ($M\Omega\ cm^2$)	V_{corr} (mm/year)
0	-0.18	2.6×10^{-11}	4.2×10^{4}	167.8	3.0×10^{-7}
50	-0.31	4.3×10^{-10}	2.6×10^{3}	143.9	5.0×10^{-6}
100	-0.49	5.3×10^{-10}	2.0×10^{3}	121.8	6.1×10^{-6}

Table 2.

Experiment condition		E_{corr} (V)	I_{corr} ($A \cdot cm^{-2}$)	R_p ($M\Omega\ cm^2$)	R_{ct} ($M\Omega\ cm^2$)	V_{corr} (mm/year)	CPE (μF)
-	0d	-0.18	2.6×10^{-11}	4.2×10^{4}	167.8	3.0×10^{-7}	4.3×10^{-4}
60.0℃	10d	-0.24	1.7×10^{-10}	1.4×10^{4}	156.1	1.9×10^{-6}	2.1×10^{-4}
-20.0℃	10d	-0.20	4.8×10^{-11}	2.3×10^{4}	159.2	5.6×10^{-7}	5.7×10^{-4}

Table 3.

Damage condition		E_{corr} (V)	I_{corr} ($A \cdot cm^{-2}$)	R_p ($M\Omega\ cm^2$)	R_{ct} ($M\Omega\ cm^2$)	V_{corr} (mm/year)	Reference
-	0d	-0.18	2.6×10^{-11}	4.2×10^{4}	167.8	3.0×10^{-7}	Present work
pH=1.0	10d	-0.24	5.8×10^{-10}	1.8×10^{3}	156.9	6.7×10^{-6}	
pH=14.0	10d	-0.21	4.6×10^{-11}	2.2×10^{4}	159.7	5.0×10^{-7}	
NaCl	10d	-0.22	9.4×10^{-11}	1.2×10^{4}	158.6	1.1×10^{-6}	
NaCl	0d	-0.84	5.3×10^{-11}	-	0.84	-	[32]
NaCl	0d	-1.5	3.3×10^{-9}	-	9.9	-	[18]
NaCl	0d	-0.29	8.7×10^{-8}	0.514	1.1	1.2×10^{-2}	[20]
NaCl	0d	-0.51	5.7×10^{-8}	-	68.5	-	[33]
NaCl	0d	-0.25	1.2×10^{-7}	-	0.18		[34]
pH=2	0d	-0.46	2.3×10^{-4}	-	4.6×10^{-3}	-	[19]
pH=7	0d	-0.41	2.4×10^{-4}	-	3.1×10^{-3}	-	
pH=9	0d	-0.42	5.2×10^{-4}	-	2.9×10^{-2}	-	

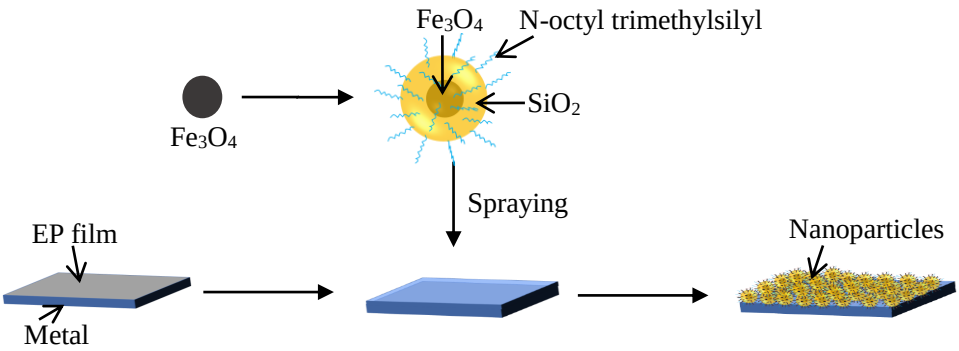
Fe3O4
Fe3O4
N-octyl trimethylsilyl
SiO2
Spraying
EP film
Metal
Nanoparticles

Scheme 1.

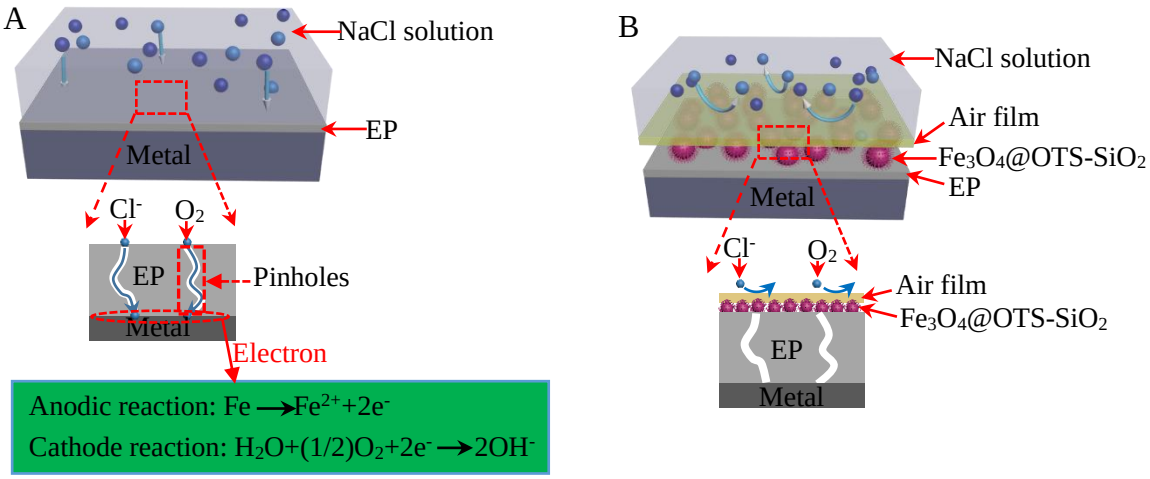
A
NaCl solution
EP
Metal
Cl-
O2
EP
Pinholes
Metal
Electron
Anodic reaction: Fe → Fe2+ +2e-
Cathode reaction: H2O+(1/2)O2+2e- → 2OH-
B
NaCl solution
Air film
Fe3O4@OTS-SiO2
EP
Metal
Cl-
O2
Air film
Fe3O4@OTS-SiO2
EP
Metal

Scheme 2.

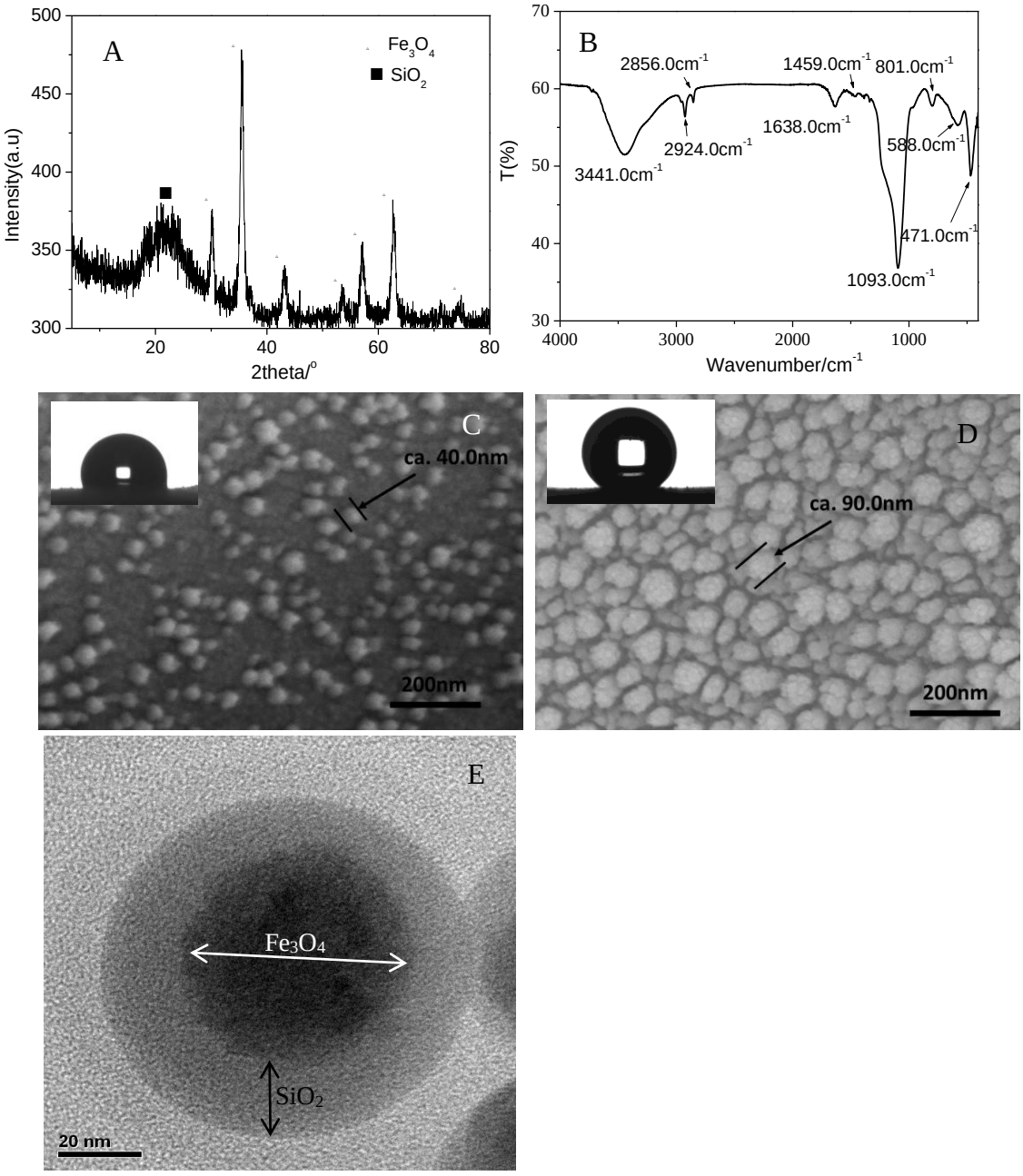
A
Fe3O4
SiO2
Intensity(a.u)
2theta/o
B
2856.0cm-1
1459.0cm-1
801.0cm-1
1638.0cm-1
2924.0cm-1
588.0cm-1
3441.0cm-1
471.0cm-1
1093.0cm-1
T(%)
Wavenumber/cm-1
C
ca. 40.0nm
200nm
D
ca. 90.0nm
200nm
E
Fe3O4
SiO2
20 nm

Fig.1.

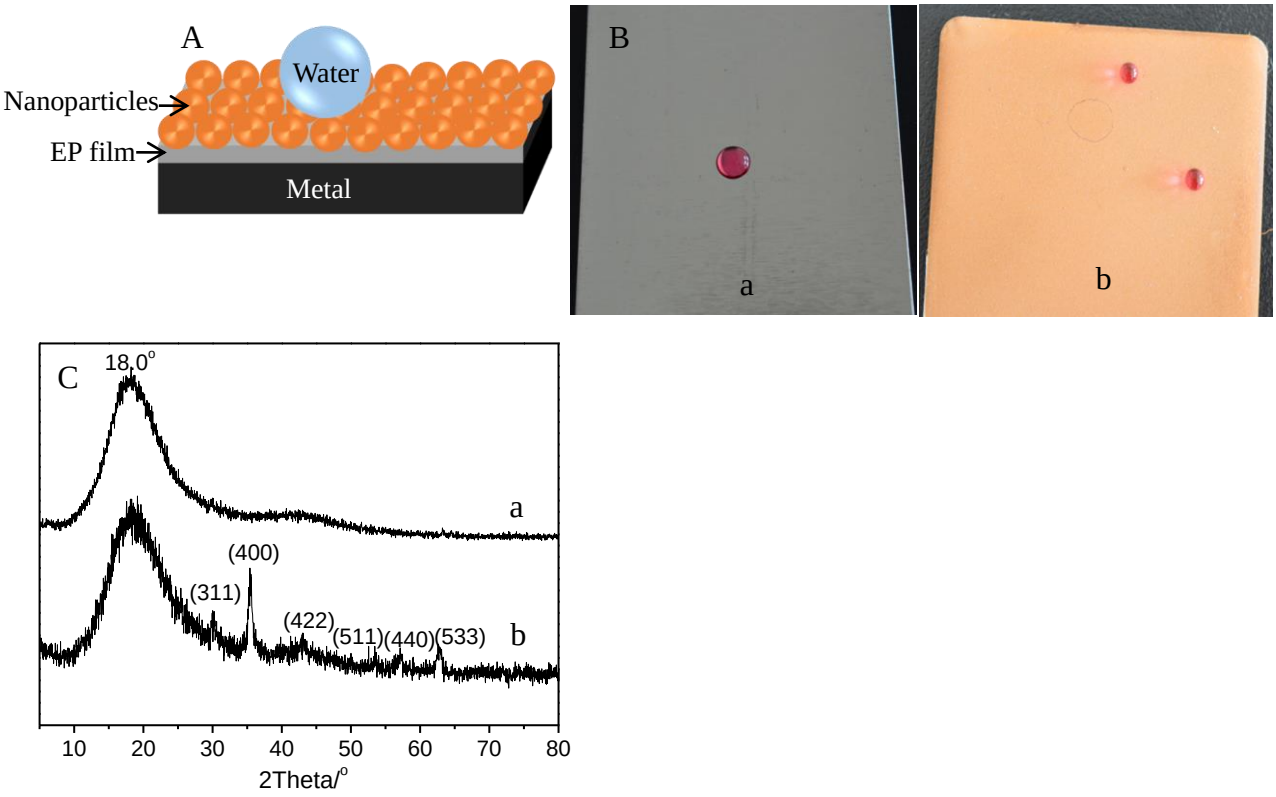
A
Water
Nanoparticles
EP film
Metal
B
a
b
C
18.0°
a
(400)
(311)
(422)
(511)
(440)
(533)
b
10
20
30
40
50
60
70
80
2Theta/°

Fig.2.

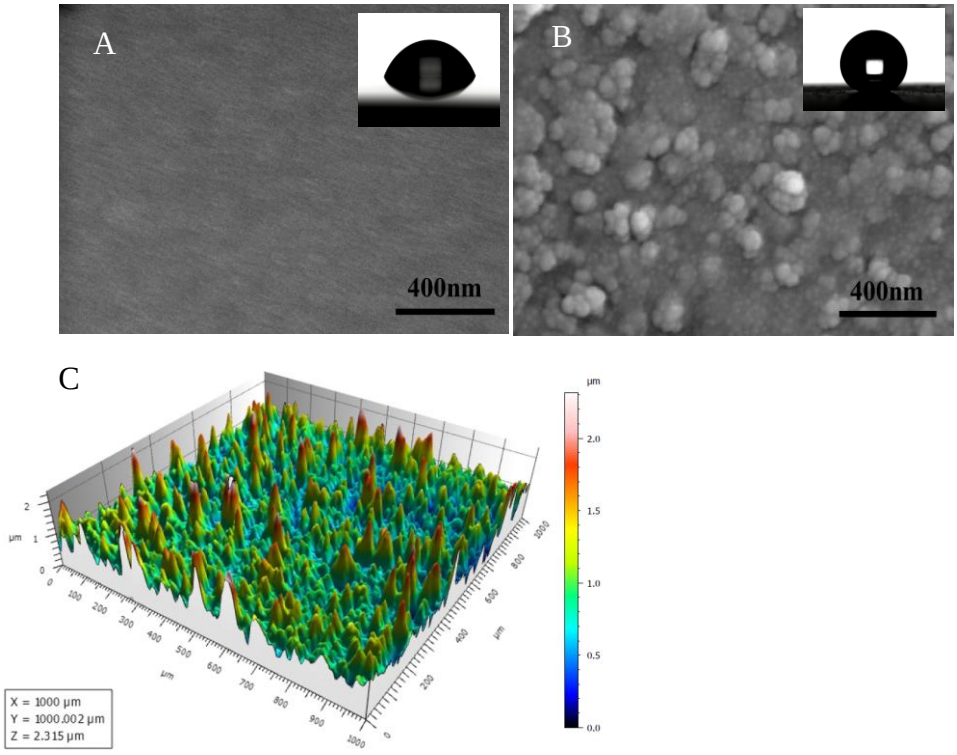
A
400nm
B
400nm
C
X = 1000 µm
Y = 1000.002 µm
Z = 2.315 µm

Fig.3.

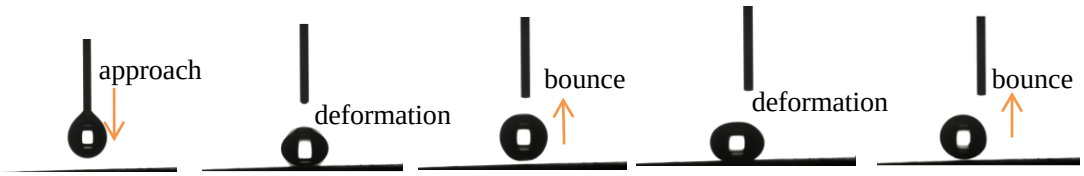
approach
deformation
bounce
deformation
bounce

Fig.4.

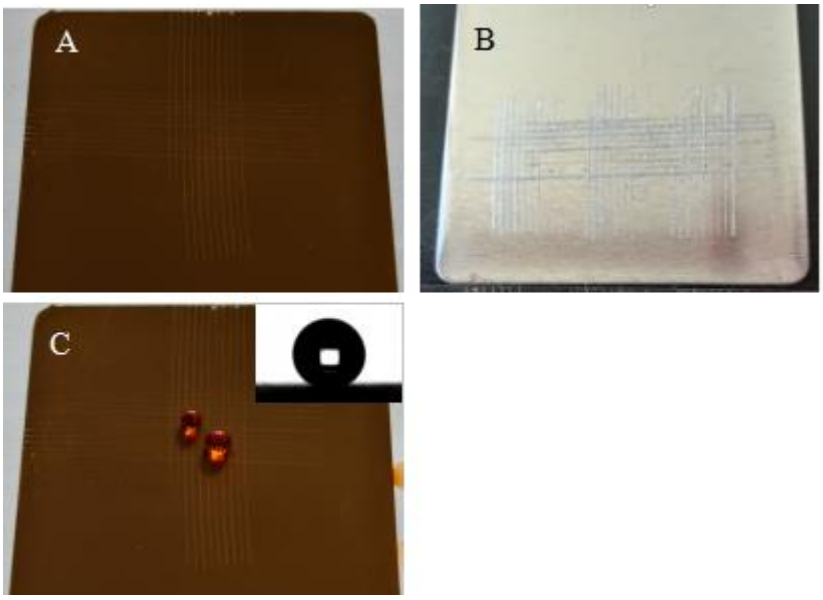

Fig.5.

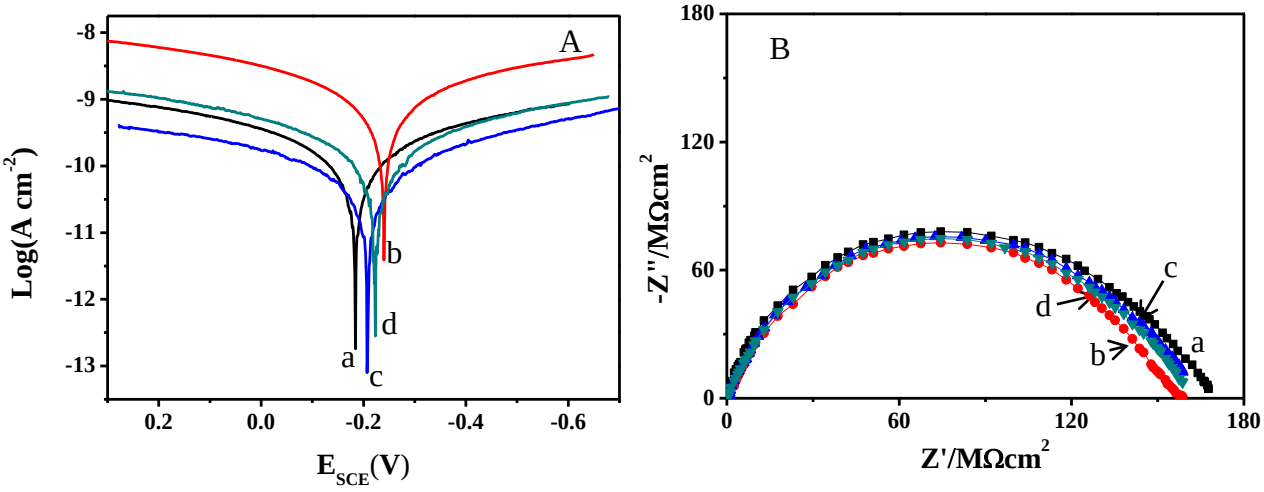
A
B
a
b
c
d
Log(A cm-2)
E SCE (V)
-Z''/MΩcm2
Z'/MΩcm2
-8
-9
-10
-11
-12
-13
0.2
0.0
-0.2
-0.4
-0.6
180
120
60
0
0
60
120
180

Fig.6.

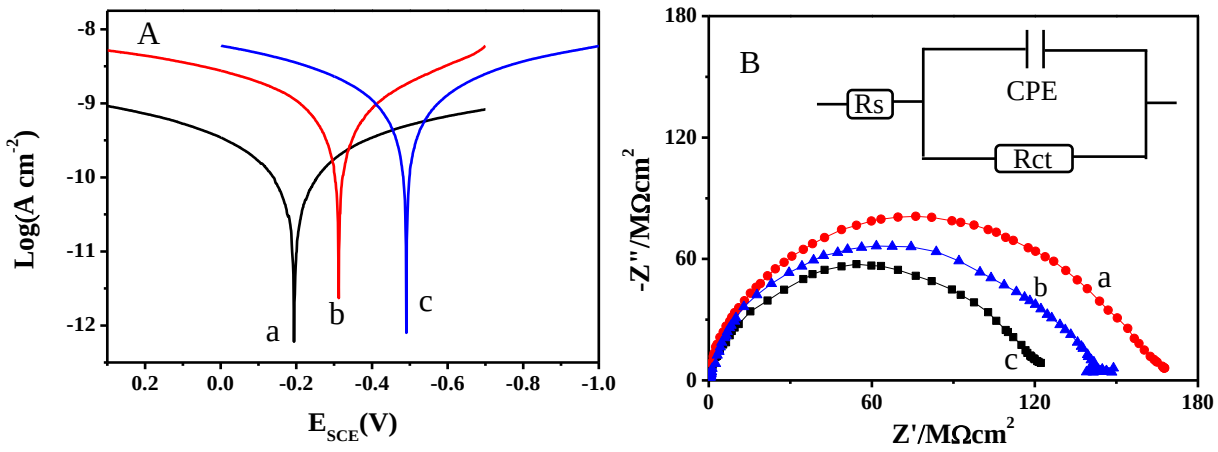
A
-8
-9
-10
-11
-12
Log(A cm-2)
0.2
0.0
-0.2
-0.4
-0.6
-0.8
-1.0
ESCE(V)
a
b
c
B
180
120
60
0
-Z''/MΩcm2
Rs
CPE
Rct
a
b
c
0
60
120
180
Z'/MΩcm2

Fig.7.

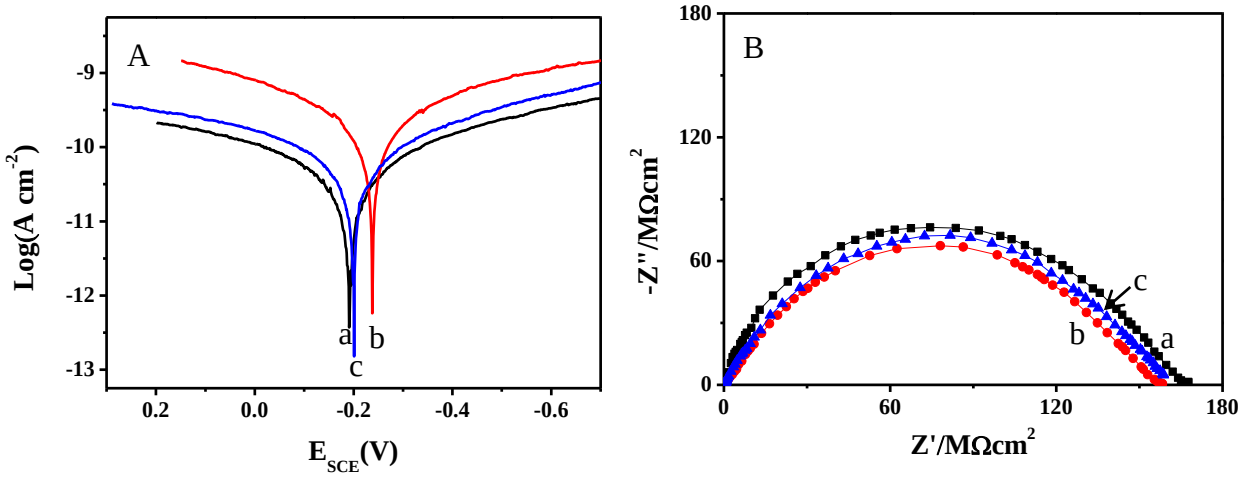
A
-9
-10
-11
-12
-13
Log(A cm-2)
0.2
0.0
-0.2
-0.4
-0.6
ESCE(V)
a
b
c
B
180
120
60
0
-Z''/MΩcm2
0
60
120
180
Z'/MΩcm2
c
b
a

Fig.8.

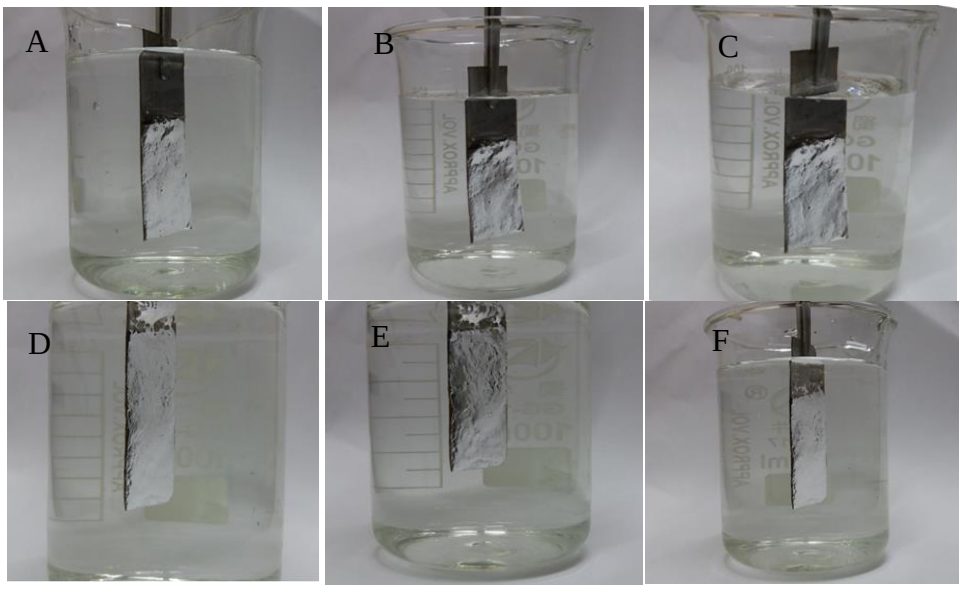

Fig.9.